Infrared transmittance spectra of the granular perovskite $La_{2/3}Ca_{1/3}MnO_3$

1998 J. Phys.: Condens. Matter 10 4315

(http://iopscience.iop.org/0953-8984/10/19/019)

J. Phys.: Condens. Matter **10** (1998) 4315–4322. Printed in the UK PII: S0953-8984(98)90660-9

Infrared transmittance spectra of the granular perovskite $La_{2/3}Ca_{1/3}MnO_3$

Kebin Li†‡, Rongsheng Cheng†, Shouguo Wang† and Yuheng Zhang‡†

† Institute of Solid State Physics, Academia Sinica, Hefei 230031, People's Republic of China
‡ Structural Research Laboratory, University of Science and Technology of China, Hefei 230026, People's Republic of China

Received 13 January 1998

Abstract. Infrared (IR) transmittance spectra were measured for a series of $La_{2/3}Ca_{1/3}MnO_3$ samples with different particle sizes. Two extra absorption peaks appear when the average particle size of the samples is smaller than 60 nm; these peaks can be ascribed to the surface stretching and bending modes of the MnO_6 octahedra. When the average particle size decreases, the absorption strength of the surface modes increases while that of the bulk modes reduces.

1. Introduction

Since the discovery of 'colossal' magnetoresistance (CMR) [1–6] in the doped manganite perovskite $Re_{1-x}Ae_xMnO_3$ (Re is a lanthanide element such as La and Nd, Ae is an alkaline-earth element such as Ca and Sr), a great deal of progress [7–10] has been made both experimentally and theoretically in explaining some intriguing physical properties found among these materials. Although the origin of the CMR effect remains unclear so far, the observed correlation between the electronic transport properties and ferromagnetism in this class of materials has been long discussed in terms of an exchange coupling mediated by the electronic hopping between neighbouring Mn e_g orbits, called the double-exchange (DE) process [11]. However, Millis *et al* [12] have pointed out that the DE model alone is not sufficient to explain the CMR effect. They proposed that a lattice distortion due to a strong electron–phonon interaction should be taken into account. The static Jahn–Teller (JT) distortion in the manganite perovskite has been confirmed by an experiment on the ^{18}O and ^{16}O isotopic effect of the Curie temperature in the compound $La_{0.8}Ca_{0.2}MnO_3$ reported by Zhao *et al* [13]. For doping levels of $x > 0.2$, although the static JT distortion is not present, it has been conjectured that the dynamic JT effect should be important [14, 15]. Experiments on the optical conductivity of $Nd_{0.7}Sr_{0.3}MnO_3$ thin films at temperatures down to 15 K and magnetic fields up to 8.9 T reported by Kaplan showed that the dynamic JT effect was indeed present [16], although no evidence of a Jahn–Teller effect was reported for $La_{0.825}Sr_{0.175}MnO_3$ by Okimoto *et al* [17].

It is well known that infrared (IR) spectra reflect the vibrating modes of the lattice in the crystal. IR phonon spectra are sensitive to local lattice distortions [15, 18]. Large frequency shifts of the internal phonon modes were observed by Kim *et al* [19] in a polycrystalline $La_{0.7}Ca_{0.3}MnO_3$ sample near the Curie temperature T_C, indicating that the electron–phonon coupling plays an important role in the lattice dynamics of the manganese oxides. This means that the exotic electronic transport and magnetic properties found for manganese

0953-8984/98/194315+08$19.50

oxides should be related to the local lattice dynamics of these compounds. Recently, some special magnetoresistive behaviours have been reported for the granular perovskites La–(Sr or Ca)–Mn–O [20–22], and in reference [22] this interesting magnetoresistive behaviour is ascribed to the coexistence of interfacial tunnelling and intrinsic transport behaviours in the system of the granular perovskite. The interfacial tunnelling effect arises from the surfaces between neighbouring grains together with the intergrain distance. Due to the large number of dangling bonds or non-coordination atoms existing in the surfaces, the lattice dynamics of the granular perovskite can be expected to exhibit new features. In this paper we report our investigations on IR spectra of a series of $La_{2/3}Ca_{1/3}MnO_3$ (LCMO) samples with different particle sizes. As the average particle size of LCMO decreases, two extra internal phonon modes which can be ascribed to surface modes appear and the absorption strength of the surface modes increases while that of bulk modes reduces.

2. Experiment

The fine particles of $La_{2/3}Ca_{1/3}MnO_3$ were prepared using the sol–gel technique with stoichiometric amounts of La_2O_3, $CaCO_3$ and $MnCO_3$ with nominal purities higher than 99.9%. First the powders were dissolved in concentrated nitric acid, resulting in a light solution. Afterwards, citric acid and ethylene glycol were added in a ratio of 4 g citric acid to 1 ml ethylene glycol and 1 g metal nitrates. The solution was heated and the excess nitric acid and water were boiled off, giving a brown gel. The gel was preheated to 300 °C to remove the remaining organic content of the gel, forming the final black–brown powder. Finally, particles of different sizes of $La_{2/3}Ca_{1/3}MnO_3$ were obtained by annealing at different temperatures, T_A. The structures of the samples were characterized using x-ray diffraction techniques (D/Max–γA). The measurements of the infrared transmittance spectra were carried out with powder samples in which KBr was used as a carrier. The mixture of LCMO powder and KBr carrier was then pressed into a slice with thickness of about 0.1 mm. The transmittance spectra were measured using a Fourier-transform IR spectrophotometer (Nico-Let 750) over the frequency range 350–4000 cm^{-1}.

3. Results and discussion

The x-ray patterns obtained for several values of T_A are shown in figure 1. Above $T_A = 400$ °C, the samples crystallize in a single phase, showing the characteristic peaks of the perovskite. The average particle size could be estimated from the x-ray linewidths, through the classical Scherrer formulation $D_{hkl} = k\lambda/B\cos\theta$, where D_{hkl} is the diameter of the particle in units of 0.1 nm, k is a constant (shape factor $\sim$0.9), B is the difference in the width of the half-maximum of the peaks between the sample and the standard sample of KCl used to calibrate the intrinsic width associated with the equipment, and λ is the wavelength of the x-rays. The photographs from the transmission electron microscope (TEM) for the samples annealed at 400 °C, 800 °C and 1000 °C are shown in figures 2(a), 2(b) and 2(c), respectively. The average particle sizes of the samples annealed at different values of T_A are summarized in table 1. This result is in good agreement with that determined by TEM.

Figure 3 shows the IR transmittance spectrum measured at room temperature for an LCMO sample sintered at 1300 °C. The peaks at 3440 cm^{-1} and 1637 cm^{-1} are of the carrier $KBr{\cdot}(H_2O)_n$. The other two strong peaks appearing at $\nu_3 = 596$ cm^{-1} and $\nu_4 = 398$ cm^{-1} should belong to the optical phonons of $La_{2/3}Ca_{1/3}MnO_3$. The x-ray diffraction result shows that the sample is of pseudo-cubic structure with a lattice parameter of 0.3876 nm. For the

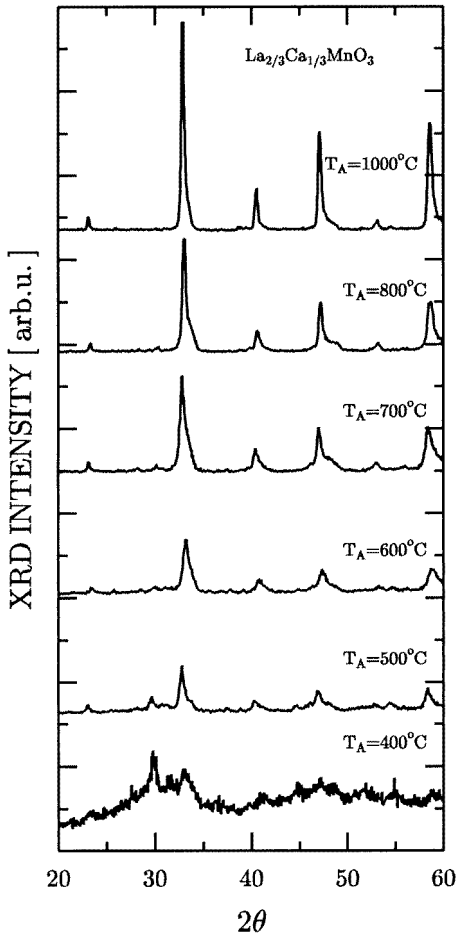

Figure 1. XRD patterns of LCMO samples at different annealing temperatures T_A.

cubic perovskite ABO_3 with the symmetry O_h^1, the normal modes of the lattice vibration at the zone centre ($k = 0, \Gamma$) are given in the irreducible representation by [23, 24]

$$\Gamma^{\text{total}} = 4F_{1u} + F_{2u}. \tag{1}$$

One of the F_{1u} modes corresponding to the acoustic phonon mode and F_{2u} is optically silent, i.e., neither IR nor Raman active. The remaining three F_{1u} modes are IR active, corresponding to the vibrational motion in which the B–O bond distance is modulated (the stretching mode), the B–O bond angle is modulated (the bending mode) or to the translational motion of the A atoms with respect to BO_3 (the external mode), as illustrated in figure 1 of reference [23]. According to the mode classification, we have assigned the two major peaks to, from low to high energy, the bending and stretching modes, respectively. The external mode appears normally below 200 cm^{-1}; this cannot be detected in our experiments. In the case of CMR perovskite, B represents the Mn element, so the stretching and bending modes represent the optical phonons of the octahedron MnO_6. In fact, $La_{2/3}Ca_{1/3}MnO_3$ has a distorted ABO_3 cubic symmetric structure. The distortion lowers the cubic symmetry, which lifts the threefold-degenerate F_{1u} (F_{2u}) modes of the cubic structure. The distortion

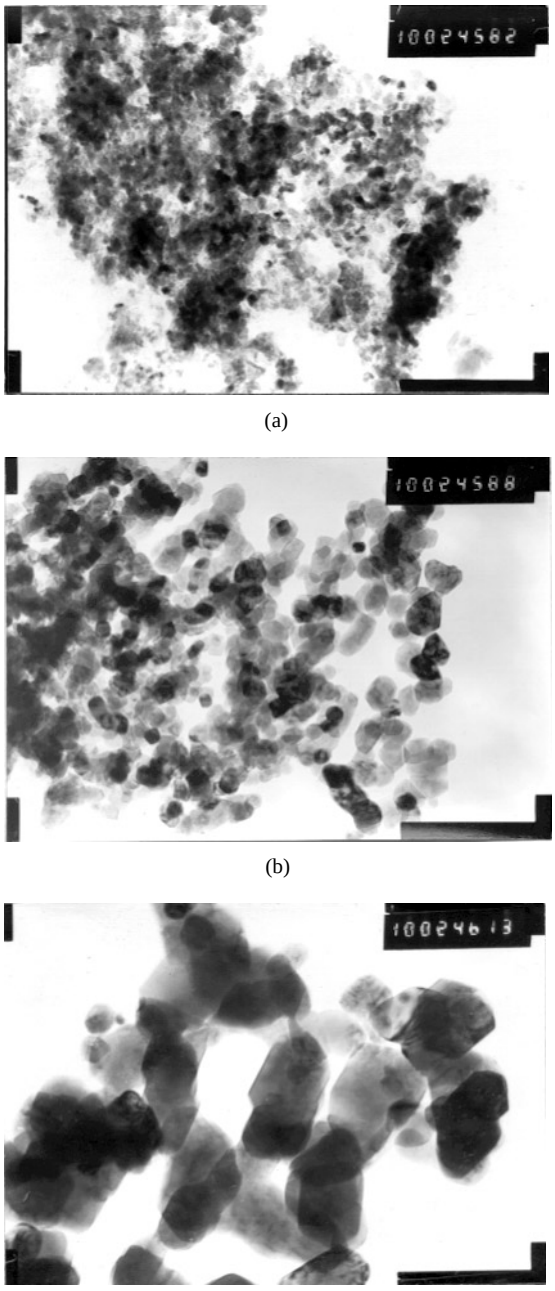

Figure 2. TEM photographs for LCMO samples annealed at 400 °C (a), 800 °C (b) and 1000 °C (c). The scale of the photographs is 1:100 000.

also enlarges the unit cell which contains more than two formula units, and as a result the phonon branches are folded into the reduced Brillouin zone, resulting in an increase in the number of Γ-point phonon modes. For example, for the perovskite-type structure

Table 1. The average particle size of $La_{2/3}Ca_{1/3}MnO_3$ at different annealing temperatures was estimated by means of the Scherrer formula through measuring the full width at half-maximum of the XRD patterns. The result is in good agreement with that determined by TEM. ν_3 and ν_4 represent the stretching and bending modes respectively.

Sample specification	TNL1	TNL2	TNL3	TNL4	TNL5	TNL6	TNL7
T_A (°C)	300	400	500	600	700	800	1000
Average particle Size (nm)	10 ± 4	10 ± 4	20 ± 5	30 ± 5	55 ± 5	70 ± 10	140 ± 10
ν_3 (cm^{-1})	518.76 582.40	518.76 582.40	511.05 582.40	520.69 586.26	512.97 595.50	595.90	595.90
ν_4 (cm^{-1})	352.00	352.00	352.00 416.55 449.34	352.00 416.55 453.19	352.00 395.34 447.41	352.00 408.84	352.00 401.13

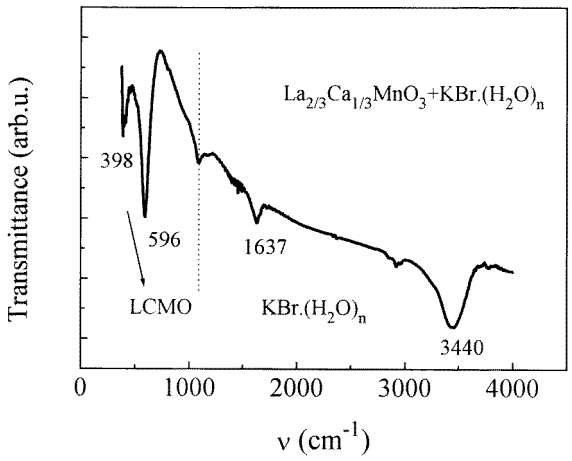

Figure 3. The IR transmittance spectrum of $La_{2/3}Ca_{1/3}MnO_3$ taken over the frequency range 350–4000 cm^{-1}.

with the rhombohedral distortion D^6_{3d} ($R\bar{3}c$), one can expect maximally eight phonons to be observable in the far-infrared spectrum. However, in the present case with the polycrystalline sample and non-polarized light, the other remaining stretching and bending modes are probably too weak to be observed in the transmittance spectrum. In fact, another obvious peak near 353 cm^{-1} has been observed; it may be ascribed to a bending mode. We do not intend to discuss it in detail because this peak is associated with an unavoidable uncertainty due to large errors at the edge of the device frequency band.

The IR spectra for LCMO samples with different grain sizes are shown in figure 4. It is obvious that there is no remarkable difference in the various aspects of the IR spectra features among the samples whose values of T_A are above 800 °C. But below $T_A = 700$ °C, both the stretching and bending modes split into two peaks. Their positions are also summarized in table 1. For example, at $T_A = 700$ °C, ν_3 splits into two peaks; one appears at 595.50 cm^{-1} and the other at 512.97 cm^{-1}. ν_4 also splits into two peaks, one at 447.41 cm^{-1} and one at 395.34 cm^{-1}. The average particle size of the sample annealed at $T_A = 700$ °C is about

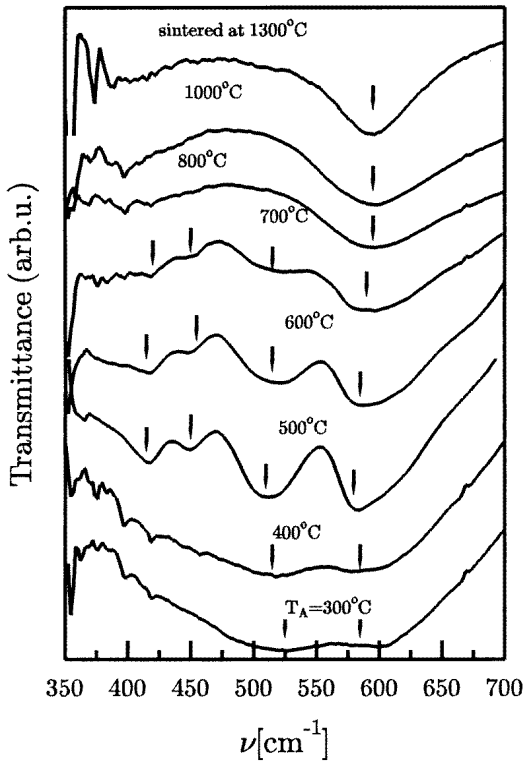

Figure 4. IR transmittance spectra of fine particles of $La_{2/3}Ca_{1/3}MnO_3$ at different annealing temperatures, T_A. The IR spectrum of $La_{2/3}Ca_{1/3}MnO_3$ polycrystalline bulk sintered at 1300 °C is also shown in the figure for comparison. The arrows hint at the positions of absorption peaks.

60 nm. Hence we believe that the peak of the stretching mode at $\nu_{3S} = 512.97$ cm^{-1} and that of the bending mode at $\nu_{4S} = 447.41$ cm^{-1} should be ascribed to the surface vibration modes. The peaks at 595.50 cm^{-1} and 395.34 cm^{-1} should still be associated with the bulk modes, i.e., $\nu_{3B} = 595.50$ cm^{-1}, $\nu_{4B} = 395.34$ cm^{-1}. As T_A is decreased, i.e., the average particle size is reduced, ν_{3S} moves to lower frequency but ν_{4S} tends to shift to higher frequency. Simultaneously, the bulk stretching mode ν_{3B} also shifts to lower frequency while the bulk bending mode ν_{4B} shifts to higher frequency. Another feature of the IR spectra of fine particles of LCMO is that the absorption strength of the surface modes increases with decreasing particle size, while the absorption strength of the bulk modes reduces, and below $T_A = 400$ °C they become comparable. It is worth noting that the bending modes disappear when T_A is below 500 °C. This phenomenon can be easily understood by assuming that the ratio of surface areas increases as the average particle size is decreased and therefore the strain increases, resulting in the suppression of the bending mode.

The surface internal phonon modes observed in the granular perovskite should be due to a large number of granular particles existing in the samples. As the particle size decreases, the number of dangling bonds or non-coordination atoms existing in the grain surfaces increases, leading to a large lattice distortion both in the grain surface and in the core; as a result, the stretching modes will shift to lower frequencies and the bending modes will shift to higher frequencies. As we stated in the introduction, there exists a strong

correlation between the electronic transport properties and ferromagnetism in the class of CMR materials. This observed correlation has been discussed in terms of a double-exchange model. In double-exchange ferromagnets, such as $Re_{1-x}Ae_xMnO_3$ perovskites, any local lattice distortion can change both the Mn–O distance d_{Mn-O} and the bending angle Θ of the Mn–O–Mn bond. Both d_{Mn-O} and Θ can affect the relevant Mn–O–Mn orbital overlap t_{ij}, which leads to a change of the electronic bandwidth W, and as a consequence, the magnetic properties of the CMR materials will influence by the local lattice distortions. Many literature examples [12–16, 19] also show that the local lattice distortion plays an important role in the electronic transport and magnetic properties of the manganese oxides. So there is no doubt that the magnetoresistive behaviour of the granular perovskites has a special nature [22]. We propose that the local lattice distortions in the grain surface as well as in the core should be considered simultaneously to interpret the magnetoresistive behaviour of the granular perovskite.

4. Conclusion

In summary, two internal phonon modes, i.e., the stretching and bending modes of the MnO_6 octahedra, were observed in a $La_{2/3}Ca_{1/3}MnO_3$ sample sintered at 1300 °C. When the average particle size of $La_{2.3}Ca_{1/3}MnO_3$ is decreased, two extra absorption peaks which can be ascribed to the surface bending and stretching modes appear. This suggests that the surface modes existing in the granular perovskite should be responsible for its special electronic and magnetic properties.

Acknowledgments

This work was supported in part by the Chinese National Natural Science Fund (No 19504012), and by the Chinese Academy of Sciences under the contract No KJ951-A1-401.

References

[1] Kusters R M, Singleton J, Keen D A, McGreevy R and Hayes W 1989 *Physica* B **155** 362
[2] von Helmolt R, Wecker J, Holzapfel B, Schultz L and Samwer K 1993 *Phys. Rev. Lett.* **71** 2331
[3] McCormack M, Jin S and Tiefel T H 1994 *Appl. Phys. Lett.* **64** 3045
Jin S, Tiefel T H and McCormack M 1994 *Science* **264** 413
[4] Ju H L, Gopalakrishnan J, Peng J L, Li Qi, Xiong G C, Venkatesan T and Greene R L 1995 *Phys. Rev.* B **51** 6143
Schiffer P, Ramirez A P, Bao W and Cheong S-W 1995 *Phys. Rev. Lett.* **75** 3336
[5] Liu J Z, Chang J C, Irons S, Klavins P, Shelton R N, Song K and Wasserman S R 1995 *Appl. Phys. Lett.* **66** 3218
Xiong G C, Li Qi, Ju H L, Mao S N, Senapati L, Si X X, Greene R L and Venkatesan T 1995 *Appl. Phys. Lett.* **66** 1427
Gupta A, McGuire T R, Duncombe P R, Rupp M, Sun J Z, Gallagher W J and Xiao Gang 1995 *Appl. Phys. Lett.* **67** 3494
[6] Sanchez R D, Rivas J J, Vazquez-Vazquez C, Lopez-Quintela A, Causa M T, Tovar M and Oseroff S 1996 *Appl. Phys. Lett.* **68** 134
[7] Arnold Z, Kamenev K, Ibarra M R, Algarabel P A, Marquina C, Blasco J and Garcia J 1995 *Appl. Phys. Lett.* **67** 2875
Moritomo Y, Asamitsu A and Tokura Y 1995 *Phys. Rev.* B **51** 16 491
[8] Xiong G C, Li Qi, Ju H L, Bhagat S M, Lofland S E, Greene R L and Venkatesan T 1995 *Appl. Phys. Lett.* **67** 3031
[9] Asamitsu A, Moritomo Y, Tomioka T, Arima T and Tokura Y 1995 *Nature* **373** 407

[10] Tokura Y, Urushibara A, Moritomo Y, Arima T, Asamitsu A, Kido G and Furukawa N 1994 *J. Phys. Soc. Japan* **63** 3931
[11] Zener C 1951 *Phys. Rev.* **82** 403
Anderson P W and Hasegawa H 1955 *Phys. Rev.* **100** 675
de Gennes P-G 1960 *Phys. Rev.* **118** 141
[12] Millis A J, Littlewood P R and Shraiman B I 1995 *Phys. Rev. Lett.* **74** 5144
[13] Zhao Guo-meng, Conder K, Keller H and Mueller K A 1996 *Nature* **381** 676
[14] Röder H, Zang Jun and Bishop A R 1996 *Phys. Rev. Lett.* **76** 1356
[15] Millis A J, Shraiman B I and Müller R 1996 *Phys. Rev. Lett.* **77** 175
Millis A J 1995 *Phys. Rev.* B **53** 8434
[16] Kaplan S G, Quijada M, Drew H D, Tanner D B, Xiong G C, Ranesh R, Kwon C and Venkatesan T 1996 *Phys. Rev. Lett.* **77** 2081
[17] Okimoto Y, Katsufuji T, Ishikawa T, Urushibara A, Arima T and Tokura Y 1995 *Phys. Rev. Lett.* **75** 109
[18] Harley R T 1977 *Electron–Phonon Interaction and Phase Transitions* ed T Riste (New York: Plenum) and references therein
[19] Kim K H, Gu J Y, Choi H S, Park G W and Noh T W 1996 *Phys. Rev. Lett.* **77** 1877
[20] Sanchez R D, Rivas J, Vazquez-Vazquez C, Lopez-Quintela A, Causa M T, Tovar M and Oseroff S 1996 *Appl. Phys. Lett.* **68** 134
[21] Mahesh R, Mahendiran R, Raychaudhuri A K and Rao C N R 1996 *Appl. Phys. Lett.* **68** 2291
[22] Zhang Ning, Ding Weiping, Zhong Wei, Xing Dingyu and Du Youwei 1997 *Phys. Rev.* B **56** 8138
[23] Tajima S, Masaki A, Uchida S, Matsuura T, Fueki K and Sugai S 1987 *J. Phys. C: Solid State Phys.* **20** 3469
[24] Fontana M D, Metrat G, Servoin J L and Gervais F 1984 *J. Phys. C: Solid State Phys.* **17** 483